Published in Surface Science 373, issues 2-3, 153-172, 1997
which should be used for any reference to this work

Growth of Ag on Cu(001) studied by full-hemispherical X-ray photoelectron diffraction

J. Hayoz *, D. Naumović, R. Fasel, P. Aebi, L. Schlapbach

Institut de Physique, Université de Fribourg, Pérolles, CH-1700 Fribourg, Switzerland

Abstract

Ag films, from the submonolayer range up to 14 monolayers (ML), have been deposited in situ on two differently cut Cu(001) single crystals. Their geometrical structure has been investigated by full-hemispherical X-ray photoelectron diffraction and by low-energy electron diffraction. Structural models developed on the basis of these data have been compared to single-scattering cluster calculations. Our results indicate the formation of a surface alloy in the initial step of the Ag growth. At coverages below 0.3 ML, we find that the local environment of the Ag atoms remains fourfold. A first indication for small quasi-hexagonal c(10 × 2) clusters, which are known to appear at 1 ML, is already observed at 0.3 ML. Ag films above 1 ML are compact and exhibit a threefold fcc (111) structure. Furthermore, we noticed that on one of the crystals one of the two possible c(10 × 2) orientations is clearly dominant, and mainly one of the four expected fcc (111) domains grows. On the other crystal the two c(10 × 2) orientations are equally present. Moreover, two fcc (111) domains rotated by 90° with respect to each other develop. We have clear evidence that, from the two possibilities of fcc (111) growth on each c(10 × 2) domain, only one occurs. The comparison of the results from the two differently cut crystals indicates that the domain population is related to the absolute miscut of the substrate and hence by the course of the steps.

Keywords: Copper; Epitaxy; Growth; Low energy electron diffraction; Metal–metal interfaces; Photoelectron diffraction; Silver; Stepped single crystal surfaces

1. Introduction

There is great interest in the study of metal–metal interfaces, because interfacial effects have a considerable influence on the magnetic, mechanical, optical and superconducting properties of thin films, mainly in multilayered structures. Studies in the field of metal-on-metal epitaxy are inspired by potential applications for optical elements that work in the soft X-ray region [1], for magnetic multilayers [2], but also for highly reaction-specific catalysts [3]. The controlled development of such complex components demands a broader understanding of the fundamental principles of crystallization phenomena of metals on metals. Hence, it is of prime importance to study the changes of the geometrical and electronic interface structure during the deposition, in particular during the deposition of the first monolayer (ML). In order to isolate some of the numerous interdependent parameters, initial research on interface structures should be performed on simple and well-characterized materials, as for instance single-crystalline noble metals (Cu, Ag, Pt, Au) [4–6].

* Corresponding author. Fax: +41 37 29 97 47;
e-mail: josef.hayoz@unifr.ch

Epitaxial films grow by different mechanisms depending, among other things, on the misfit between substrate and film, the so-called lattice mismatch (LM), on the supersaturation (flux), on the growth temperature (surface diffusion) and on the adhesion energy. The following examples illustrate the influence of LM on crystal growth:

(1) In the past years four authors independently reported on a novel kind of two-dimensional alloy [7–10]. In each of these studies it was found that a pair of elements which are immiscible in the bulk readily form a mixture confined to a single atomic layer at the surface. The common characteristic of all these systems is a big LM. In a simple theoretical work based on surface energy, on interface energy and on strain energy, Tersoff showed that such surface-confined mixing is expected quite generally in systems which are dominated by the atomic size mismatch [11].

(2) If the growth mode is of the Frank–van der Merwe (FM) or of the Stranski–Krastanov (SK) type, a large misfit between the film and the substrate may, after the deposition of the first ML, induce a structural transformation due to the strain. For instance, in the case of square (001) and rectangular (110) orientations, the deposit can prefer a pseudo-hexagonal structure. In a recent study, Naumović et al. [6] summarized observations made on seven noble-metal on noble-metal interfaces studied by full-hemispherical X-ray photoelectron diffraction (XPD). These data demonstrate first that a change of the crystalline orientation of the overlayer may occur if the LM is important and second, the strong tendency of Au to grow as a fcc (111) face on (001) oriented substrates as already reported earlier by Palmberg and Rhodin [12].

The properties of ultrathin Ag films grown on Cu(001) single crystals have attracted considerable interest in the last few years. One reason is the metallurgical simplicity of the corresponding interface. At room temperature (RT) Ag and Cu are immiscible and the interface therefore is expected to be abrupt [13,14]. Also, the Cu(001) face does not reconstruct [12]. Moreover, Ag has a much smaller surface energy (γ) than Cu ($\gamma_{Ag} \ll \gamma_{Cu}$) and one therefore expects layer-by-layer growth at least up to one complete ML. Thus one has a well-defined model system to study the interface properties. The easy preparation of the Ag/Cu(001) system and the stability of its constituents simplify experimental work. Another reason is that this interface is an experimentally convenient system for the study of dissolution kinetics at elevated temperatures [15–17]. Studies of a surface critical phenomenon associated with surface segregation in dilute Cu(Ag) bulk alloys, the so-called "surface-miscibility gap", are also a challenging field [15–19]. Due to this wide interest a lot of information on the electronic properties [20,21], on the growth mode [20–23] and on the atomic geometry [5,6,12,14,20–26] of Ag on Cu(001) single crystals is available.

In the present work 22 Ag films, from the submonolayer range up to 14 ML, have been deposited in situ on two differently cut Cu(001) single crystals at RT. Due to the big LM of 13.2%, one of our main interests in this study was to check if the formation of a surface-confined alloy occurs at RT. In order to get information on the nucleation process the structure of very thin Ag films (<0.3 ML) has been investigated. Moreover we have estimated the population of the two possible c(10 × 2) domains observed between 0.3–1 ML and of the four possible fcc (111) domains occurring for thicker Ag films (>1 ML) [5,6].

The structure of the deposited Ag films has been investigated by low energy electron diffraction (LEED) and by XPD presented as full solid-angle intensity maps, so-called diffractograms. Both methods are very sensitive to the top few surface layers. While LEED probes the long-range order, full-hemispherical XPD [27] is very sensitive to short-range structural order near the surface. XPD is particularly attractive for structural investigations of adsorbate systems, surface reconstructions, epitaxial growth or ordered surface alloys [4–6,28]. At electron kinetic energies above 500 eV, the strongly anisotropic scattering of the electrons by the ion cores leads to a forward focusing of electron flux along the emitter-scatterer axis [29–31]. In this energy range the development of atomic rows and dense crystal planes as a function of coverage Θ can easily be followed by full-hemispherical XPD. Contrary to LEED, which shows

the symmetry of reciprocal-space, XPD data contains direct real-space information.

2. Experimental procedures

The experiments were performed in a Vacuum Generators ESCALAB Mark II spectrometer modified for motorized sequential angle-scanning data acquisition [27], equipped with a three-channeltron detection system and with a base pressure in the low 10^{-11} mbar region. Photoelectron spectra and diffraction patterns were measured using Si Kα ($h\nu = 1740.0$ eV) radiation. All XPD and LEED experiments were performed at RT.

Two different Cu(001) crystals were used. Their miscut and its absolute azimuthal direction with respect to the crystal lattice was determined by a combination of Laue diffraction and laser reflection to within $\pm 0.05°$ and $\pm 5°$ in azimuth, respectively [5]. The crystal which we will label hereafter **Cu*(001)** appeared to be miscut by 0.65° along the $[\bar{1}10] \rightarrow [1\bar{1}0]$ direction (ascending steps) (Fig. 1a). The other crystal was found to be miscut by 0.55° along the $[\bar{1}00] \rightarrow [100]$ direction. This crystal we simply call **Cu(001)** (Fig. 1b). If one considers monoatomic steps and equal terrace lengths, the average terrace length is in the first case of the order of 160 Å, and in the second of the order of 190 Å. Several scanning tunneling microscopy (STM) studies found monoatomic steps on Cu(001) crystals running in ⟨110⟩ directions [32,33]. Therefore one can expect the steps in the first case to be straight and parallel and in the second case to be serrated (Fig. 1).

Clean surfaces, i.e., with C- and O-contaminants lower than 2% of a ML, were prepared by cycles of 1 keV Ar^+ sputtering and annealing to 800 K. Care was taken to ensure that the Cu(001) samples reached RT before Ag deposition. Ag was deposited from a liquid-nitrogen cooled hot-filament evaporator using a tantalum wire, at pressures below 3×10^{-9} mbar. LEED pictures at different energies were taken for each coverage Θ. The coverage (Ag 3d Cu 3p ratio) as well as the purity of the deposited Ag layers were determined by core-level photoemission. After Ag deposition the O-contamination never exceeded 0.05 ML and the C-coverage was always lower than 0.02 ML.

The sample was then transferred in situ to a two-axis goniometer which enables sweeping the photoelectron emission direction over the whole hemisphere above the surface by computer-controlled crystal rotation. For each Ag coverage diffractograms of the Ag $3d_{5/2}$ ($E_{kin} = 1371.9$ eV) and the Cu $2p_{3/2}$ emission ($E_{kin} = 807.8$ eV) were measured. The data acquisition procedure for obtaining these diffractograms consists in measuring series of azimuthal (ϕ) scans, at polar angle intervals of $\Delta\theta = 2°$. It begins at $\theta_{start} = 88°$ off normal and terminates at $\theta_{end} = 0°$. The azimuthal angular step size at any polar angle is chosen such that the solid-angle sampling density is uniform. Finally, the two-dimensional data $I(\theta,\phi)$, containing 5044 different angular settings, are visualized in the form of a gray-scale image through a stereo-

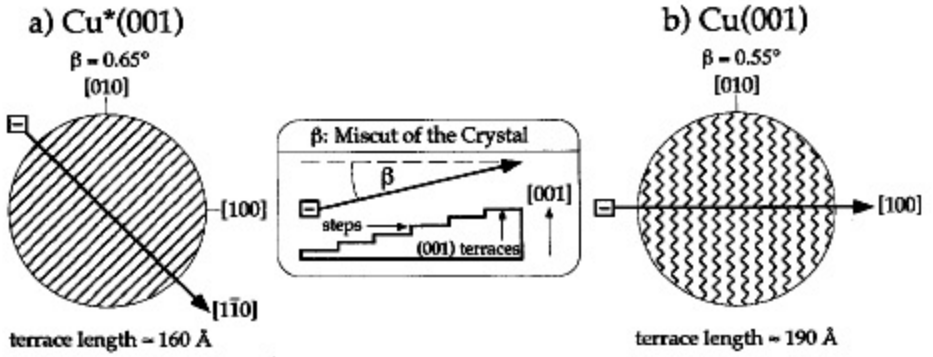

Fig. 1. Miscut β and its absolute direction with respect to the crystal lattice for (a) **Cu*(001)** and (b) **Cu(001)**. The expected terrace length is given and the expected shape of the resulting steps is sketched [5].

graphic projection [27]. Typical data acquisition times were 8 hours at a pressure of 4×10^{-11} mbar. During this time contamination levels remained unchanged.

In order to facilitate the discussion of the data we show in Fig. 2 the stereographic projection of the main low-index directions and high-density crystal planes of a fcc (001) (Fig. 2a) and a fcc (111) (Fig. 2b) crystal surface. Note that the center of the circle corresponds to the surface normal while the outer circle represents angles parallel to the surface, i.e., 90° off normal. All

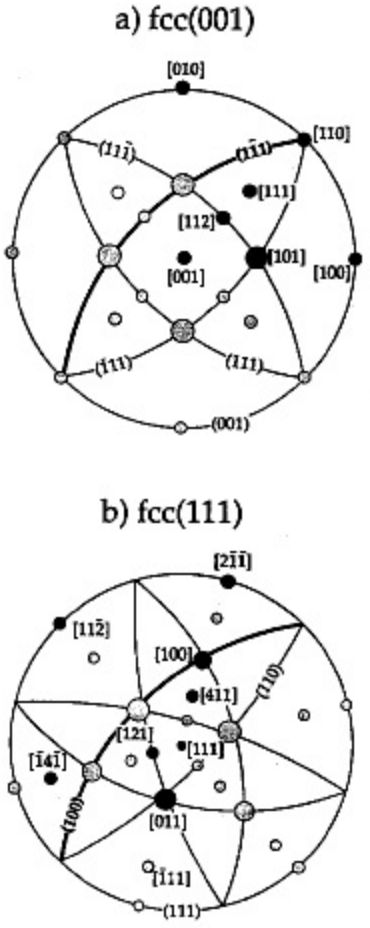

Fig. 2. Real-space stereographic projection of some low-index crystal directions (spots) and high-density planes (lines) for a fcc (001) (a) and a fcc (111) (b) crystal surface serving as a guide for diffractograms shown in this work. The labeled low-index directions correspond to the black spots. Shaded spots represent equivalent directions. The bold lines indicate high-density planes common to both surfaces.

Ag $3d_{5/2}$-diffractograms we present in this study are oriented such that the [100] direction of the underlying Cu(001) crystal points to the right-hand side as it is the case in Figs. 1 and 2a.

Let us introduce abbreviations for the different representations of the XPD patterns used in this study.

(1) "npa" (normalized with phi-average): in order to eliminate the smooth polar-angle dependence of the photoelectron intensity typical for adsorbate emission [4], the patterns in this representation are normalized with respect to the mean intensity for each polar emission angle.

(2) "2s" or "4s" (2-fold or 4-fold symmetry-averaging): to improve statistics the patterns are azimuthally averaged exploiting the 2-fold or 4-fold rotational symmetries of the corresponding systems.

(3) "rc80" (ring cut at $\theta = 80°$): neglects all data points with $\theta > 80°$. In the case of emission from thick films ($> \sim 2$ ML) the long path the photoelectrons have to travel before leaving the overlayer results in a strong damping of the photoelectron intensity for $\theta > 80°$. This low intensity dominates the dynamic range of the gray-scale image. Hence, the "rc80" representation is mainly useful for substrate-emission or for emission from thick films.

The specific combination of these three procedures used to present the XPD data is indicated in each figure.

To understand and interpret the XPD patterns we performed numerous single-scattering cluster (SSC) calculations. Details of the SSC calculation scheme used to model the photoelectron diffraction data are described elsewhere [4,5,27,28,34]. A circular, two Cu-layer thick Cu(001) basis cluster with a diameter of 25.5 Å was used to represent the Cu surface. By substituting Cu atoms with Ag atoms and/or by adding Ag atoms to this cluster we could easily simulate the supposed atomic arrangements present on the surface after Ag deposition. A R-factor, R_{MP}, based on the space of multipole expansion coefficients of the diffractograms was used to judge the comparison between experimental and simulated diffraction data [28].

To model the growth of Ag on Cu(001) crystals, an exact knowledge of the quantity of Ag deposited on the Cu(001) surfaces is helpful. The thickness

of the deposited films was estimated by comparing the intensity of the overlayer Ag 3d core-level peak with that of the substrate Cu 3p peak. If one assumes that the overlayer is homogeneous and takes into consideration the inelastic mean free path of the photoelectrons in the substrate and/or in the overlayer [35], one can determine the number of deposited ML. The following considerations show that our calibration is reliable. Ref. [6] indicates that thick Ag films are compact, i.e., the substrate is completely covered with Ag. Therefore the assumption of a homogeneous film is reasonable. For both crystals, a plot (not shown) of the Ag 3d photoelectron intensity versus the evaporation time exhibits an abrupt increase of the slope at around 0.9 ML. As discussed in Refs. [20,36] this is expected for systems which grow in a layer-by-layer mode. From the literature it is known that Ag grows on Cu(001) crystals in the FM [20,23,25] or in the SK [22] mode. On the other hand, it is well known that the first complete Ag layer exhibits a $c(10\times2)$ structure with 9 Ag atoms for every 10 Cu atoms [12]. The first complete Ag-layer therefore corresponds to a coverage of 0.9 ML.

3. Results and discussion

3.1. Thin films ($\Theta < 0.75$ ML)

For coverages below 0.5 ML no data are available in the literature, and therefore the nucleation of Ag growth on Cu(001) crystals is unknown. From our experiments, neither XPD nor LEED revealed any significant differences in the structures of Ag films deposited on the two differently cut Cu(001) crystals for coverages below 0.3 ML.

After deposition of a 0.05 ML thick film the LEED pattern remains unchanged, i.e., only (1×1) substrate spots are visible (Fig. 3a). This observation allows two interpretations: Either the deposited Ag atoms are randomly distributed over the surface, or possibly ordered clusters are still to small to produce diffraction spots. A LEED pattern taken from a 0.2 ML thick Ag film is shown in Fig. 3b. Note that LEED and XPD patterns are not oriented identically. In addition to the (1×1)-substrate spots one observes several streaked spots. In reciprocal space all these streaks are parallel either to the [10] or to the [01] direction and must be caused by disorder along the $[\bar{1}10]$ or the [110] direction in real space. One possible type of disorder is incoherent displacements between adjacent overlayer rows [37]. In this case the streaks would indicate the formation of rows of Ag atoms along either the [110] or the $[\bar{1}10]$ direction. At a Ag coverage of 0.35 ML the LEED spots are still elongated, but compared with those observed at 0.2 ML (Fig. 3b) the streaking is less pronounced. Moreover, the background is less diffuse. Apparently, with increasing Ag coverage the displacements between adjacent overlayer rows become more and more regular, and the Ag clusters get more and more ordered and compact. Finally, at a Ag coverage of 0.5 ML all LEED reflexes are sharp (Fig. 3c). Note that they remain nearly unchanged up to a coverage of 1.6 ML. Bauer [26] and Palmberg et al. [12] observed the same LEED pattern at a Ag coverage of 1 ML. They explained the observed LEED reflexes with a quasi-hexagonal $c(10\times2)$ reconstruction, which can occur in two orientations rotated by 90° with respect to each other.

In Figs. 3d and 3e we present the XPD results of 0.05 ML and 0.20 ML thick Ag films, respectively, both in the "4s.npa" representation. These patterns exhibit a 4-fold symmetry. The strong forward-focusing maxima along the four ⟨110⟩-type directions (see Fig. 2a) indicate the directions of nearest neighbors around the Ag emitters. The next-nearest neighbors are recognized in the four ⟨100⟩ directions. Furthermore, faint intensity maxima are seen at 45° polar emission angle along the four ⟨101⟩-type directions. The observation of maxima along the four ⟨101⟩ directions at these very low coverages is incompatible with a two-dimensional Ag overlayer. As the growth mode of Ag on Cu(001) is known to be of the FM or SK type [20,22,23,25], this result indicates the presence of Ag emitters within or below the Cu surface. Moreover, the XPD maps exhibit several fine features of enhanced intensity. Square-like features are formed by lines connecting the four ⟨110⟩ peaks, and four weaker lines link the four ⟨100⟩

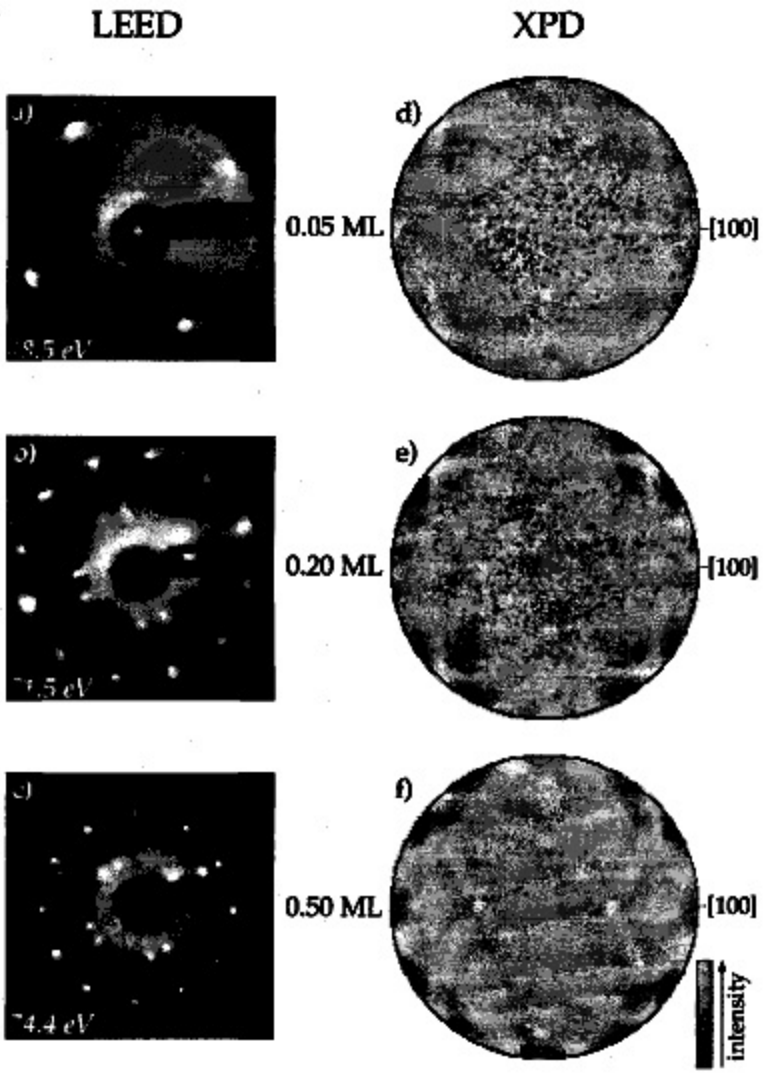

Fig. 3. LEED patterns and stereographic projection of Ag $3d_{5/2}$ diffractograms ($E_{kin} = 1371.9$ eV) in the "4s.npa" representation for different Ag coverages on Cu(001). Note that LEED and XPD patterns are not oriented identically. LEED: (a)–(c), energies are labeled; XPD: (d)–(f).

maxima. Finally, the comparison with Fig. 2a shows that an additional set of very faint lines is visible at the location of the four {111}-like planes of Cu(001). To check if this last type of line and the four maxima in the ⟨101⟩ directions could be a background effect caused by the strong Cu(001) substrate signal, we measured a diffractogram of the clean Cu(001) surface at the kinetic energy corresponding to the Ag $3d_{5/2}$ emission line. In the resulting XPD map no structure at all was visible. Therefore the features in question are not an experimental artefact. In Fig. 3f we display the Ag $3d_{5/2}$ diffractogram of a 0.5 ML thick Ag film in the "4s.npa" representation. Compared to the diffractograms of thinner Ag films (Figs. 3d and 3e) the four ⟨100⟩-like forward-focusing maxima "split off" into eight intense peaks located at very grazing angles, about 30° away from the four ⟨110⟩ maxima. Moreover, the four faint lines which linked the four ⟨100⟩ maxima at lower

coverages disappeared. By contrast one still observes intense maxima along ⟨110⟩, the faint peaks along ⟨101⟩ and the other lines already described for very thin films.

The XPD map of the 0.05 ML thick Ag film (Fig. 3d) can be explained assuming three kinds of Ag atoms on the Cu(001) surface (Fig. 4a): (i) Ag atoms in hollow sites, (ii) Ag atoms in substitutional sites and (iii) Ag atoms in substitutional sites with a Ag atom in the overlying hollow site. We suppose that, similar to the case of submonolayer Fe inclusions in Cu(001) [38], Ag atoms of type (ii) develop by Ag–Cu exchange. Moreover, when a diffusing Ag atom meets an embedded Ag atom it may be trapped in the overlying hollow site. The result of this trapping process is a Ag atom of type (iii). For each of these three cases we appropriately modified the basis cluster described above and performed SSC calculations. From Fig. 4a one sees that Ag atoms of type (ii) yield the four strong ⟨110⟩ (nearest neighbors) and the four less intense ⟨100⟩ (next-nearest neighbors) maxima. To obtain the ⟨101⟩ maxima as well, one has to take into consideration Ag atoms of type (iii). The intensity distribution resulting from emission from Ag atoms located in hollow sites (type (i)) is important to reproduce the square-like line structures observed in the experimental data. Finally, we added up these three contributions with different weights. The weights (i):(ii):(iii)=6:1:2 (Fig. 4a) yield the best agreement between the calculated data and the experiment (Fig. 3d). Only the four very faint lines running analogous to the stereographic projections of the four {111}-like planes of a fcc (001) crystal (Fig. 2a) are missing. According to this qualitative result, 33% of the deposited Ag atoms are substituted into the first Cu layer at the lowest coverage of 0.05 ML, 11% corresponding to type (ii) and 22% corresponding to type (iii). Note, that the ⟨110⟩ and ⟨100⟩ maxima could also be explained by having several Ag atoms in adjacent hollow sites without Ag atoms in substitutional sites. With this configuration, however, the ⟨101⟩ maxima would not be reproduced. Moreover, all the experimental features described above can also be simulated by SSC calculations using a model with some Ag atoms substituted into the first Cu layer and, in addition, a very small number of Ag atoms in the second Cu layer. Based on the present experiments, however, it is not possible to distinguish Ag atoms substituted in the first Cu layer with a Ag atom in the overlying hollow site from Ag atoms substituted into the second Cu layer. Hence, the number of Ag atoms substituted within the second Cu layer cannot be estimated.

In a STM study, McMahon et al. [39] examined the structure of submonolayer Ag deposits on Cu(111). Apparently the long diffusion length of Ag – the substrate temperature during deposition was about 100°C – leads to the formation of large (111)-like islands nucleating at the downhill side of the Cu step edges. Even for Ag deposition at RT on Cu(001), Ag atoms may behave similarly and stick to the downhill side of the Cu step edges. With our XPD data, however, we cannot determine if Ag nucleates on the terraces or at the downhill side of the Cu step edges. To learn more about the nucleation process we plan to combine XPD studies with STM.

We propose the following tentative model of the nucleation process: During deposition the Ag atoms are randomly distributed on the Cu(001) surface. Some Cu atoms are substituted by Ag atoms. Most of the Ag atoms diffuse across the Cu surface until they are trapped at the downhill side of the step edges, or, until they meet a substituted Ag atom and are trapped in one of the overlying hollow sites. The steps and the substitutionally adsorbed Ag atoms therefore act as nuclei for the formation of small Ag islands, still preserving in average the local fourfold symmetry.

XPD reveals that the local environment of the Ag atoms remains fourfold below 0.3 ML. The first little Ag clusters therefore have to be fourfold. Based on the ratio of the lattice constants ($a_{Ag}/a_{Cu}=1.133\approx1.125=9/8$) we propose a pseudoepitaxial c(9×9) structure. Due to the lateral displacement of the Ag atoms with respect to the Cu surface-lattice this structure would be very corrugated and its unit cell would be dome-like with a square base of eight Ag atoms (see Ref. [25]). Note that at this very low coverage the size of these clusters would be much smaller than one complete c(9×9) unit cell (Fig. 4b). According to our nucleation model the clusters

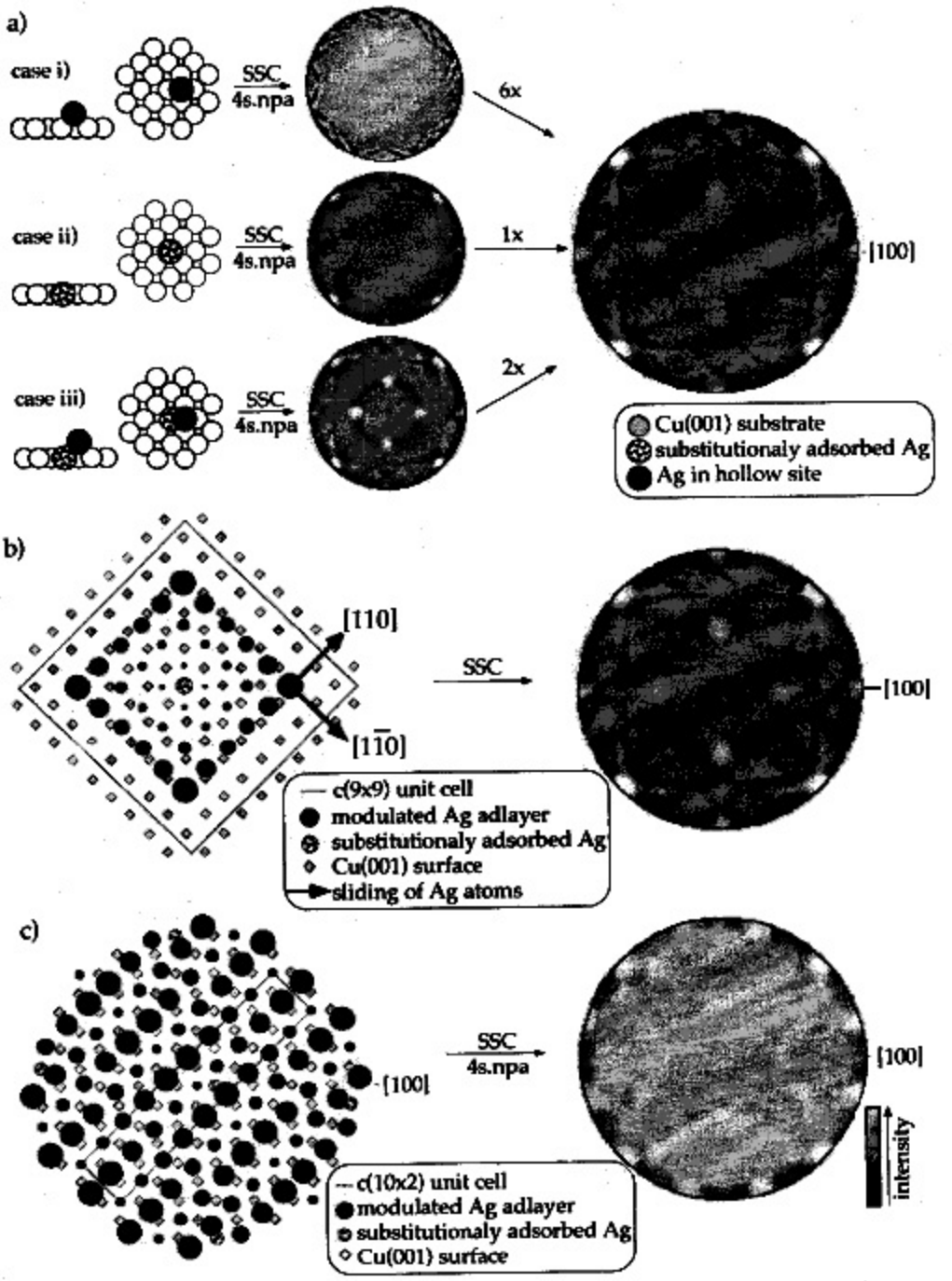

Fig. 4. (a) At the very beginning of the Ag growth there are essentially three kinds of Ag atoms at the surface (see text). The corresponding results from SSC calculations are shown in the "4s.npa" representation. The diffraction pattern on the right hand side is obtained by summing up the three contributions. (b) We suppose the first little Ag clusters to have a strongly corrugated 4-fold symmetric c(9×9) structure. The modulation is indicated by different sizes of the dots: higher positions correspond to larger dots. The SSC calculation shown corresponds to a cluster size of 36 Ag atoms centered around the substituted Ag atom (see text). (c) Modulated c(10×2)-Ag/Cu(001) layer ([110]-domain). This structure results when Ag atoms populating c(9×9) clusters start to slide along the ⟨110⟩ directions (see text). In the SSC calculation we did account for both 90°-rotated orientations and for the nine inequivalent sites the substituted Ag atom can occupy with respect to the Ag adlayer (see text).

start growing from the Ag atoms substituted into the first Cu layer, which therefore have a well-defined and unique position with respect to the overlying c(9×9) cluster. The result of the SSC calculation using this structure is presented in Fig. 4b. Again the simulation reproduces the experimental features (Fig. 3e) very nicely.

In a theoretical work Mottet et al. [25] discussed the c(9×9) structure described above. They calculated the variation of the adsorption energy with coverage for the Ag/Cu(001) system and found two minima corresponding to two kinds of superstructures: (i) the pseudo-hexagonal c(10×2) reconstruction at a coverage of 0.90 ML and (ii) the pseudoepitaxial c(9×9) structure at a coverage of 0.79 ML. An experimental hint for the existence of a superstructure at coverages lower than 0.6 ML has been given by Eugène et al. [17]. They studied the influence of the surface orientation on the equilibrium superficial segregation of silver on copper, comparing the dissolution kinetics of the (111), (110) and (001) surfaces at 450°C. To explain the observed behavior for the (001) surface for Ag coverages below 0.6 ML they proposed the existence of a not yet observed superstructure. Up to now, however, neither the proposed c(9×9) nor any other structure has been observed at very low Ag coverages in an experiment. This is not surprising. As mentioned above, such c(9×9) clusters appear to be very corrugated and their structure might therefore be quite unstable. Playing with little metallic balls suggests that at a cluster size of about 36 Ag atoms, i.e., much smaller than the size of one c(9×9) unit cell, the Ag atoms tend to slide along the ⟨110⟩ directions (Fig. 4b), building Ag rows running along ⟨110⟩ (see Fig. 4c). The result of this structure transformation is the well-known, less-corrugated and more-compact c(10×2) superstructure which can occur in two equivalent orientations rotated by 90° with respect to each other. Considering such small c(9×9) clusters and the sliding of the Ag atoms along ⟨110⟩, the streaks observed with LEED (Fig. 3b) can be understood as due to incoherent displacements between adjacent overlayer rows.

Fig. 4c shows one domain of the quasi-hexagonal c(10×2) reconstruction with Ag rows along [110]. Hereafter we will call this orientation "[110]-domain", and the orientation with Ag rows running along [$\bar{1}$10] will be labeled "[$\bar{1}$10]-domain". Adjacent Ag rows are displaced by a nearest-neighbor distance of the underlying Cu(001) substrate. The fact of having 9 Ag atoms for every 10 Cu atoms along the Ag rows implies the existence of many inequivalent sites, and therefore a corrugation of the adlayer along the rows. The maximum modulation amplitude was determined to be of the order of 0.15 Å [12,25]. Note that the quasi-hexagonal c(10×2) structure is much less corrugated than the pseudoepitaxial c(9×9). The cluster used to simulate this c(10×2) structure is shown in Fig. 4c. Taking the second 90°-rotated orientation into account, the total of twelve spots appearing at grazing emission can be explained without considering any substituted Ag atoms. However, the four lines running analogous to the stereographic projection of the four {111}-like planes of a fcc (001) crystal (Fig. 2a) are missing. Replacing the Cu atom in the cluster center with a Ag atom reproduces these lines, but their shape is not continuous as is the case in the experiment (Fig. 3f). Analogous to the case of c(14×2) Au/Cu(001) growing on a Au substituted Cu(001) surface [4,5], the substitutionally adsorbed Ag atoms can occupy nine different inequivalent sites with respect to the c(10×2) unit cell, and therefore one has to take into account all the nine different configurations. Indeed, after adding up the nine resulting contributions for both possible domains the shape of the lines becomes continuous (Fig. 4c). Moreover, our simulations were best for a modulation amplitude of 0.15 Å, in agreement with Palmberg et al. [12]. A comparison of the calculated data (Fig. 4c) with the experiment (Fig. 3f) shows, that our simulation is excellent.

One could wonder why we already clearly observe the c(10×2) reconstruction at 0.3 ML with XPD and at 0.5 ML with LEED, while other authors report that it occurs at a coverage of about 1 ML Ag [12,20–23,26]. Probably the most close-packed structure is the most stable one, meaning that, even for low coverages, the Ag layer structure is made of c(10×2) islands which grow in size with increasing coverage. Indeed, the lowest background and the sharpest c(10×2) LEED reflexes are observed around 0.9 ML. This cover-

age corresponds to one complete c(10×2) Ag layer. With further Ag deposition the intensity of the twelve LEED spots near the border of Fig. 3c remains unchanged, but, due to the formation of the second Ag layer, the spots in the center fade out (see below).

To explain several features observed in the Ag $3d_{5/2}$ diffractograms of thin films ($\Theta < 0.75$ ML) we had to substitute Ag atoms into the first Cu layer, thus forming a surface alloy (Fig. 4a). There are essentially three kinds of Ag atoms at the surface (Fig. 5a): (i) Ag atoms in hollow sites, (ii) Ag atoms in substitutional sites and (iii) Ag atoms in substitutional sites with a Ag atom in the overlying hollow site. In the following, their relative contribution to the observed diffraction pattern is quantified using a simple model. We suppose that the photoelectron intensity I of the unscattered spherical waves emitted by these three kinds of Ag atoms is equal. To estimate the extent of the surface alloying at RT we neglect the intensity contribution of the Ag atoms in substitutional sites without an atom in the overlying hollow site (case (ii)). The photoelectron intensities emitted along ⟨101⟩, $I_{\langle 101\rangle}$, and the one emitted in all other directions, I_{off}, can be written as follows:

$$I_{\langle 101\rangle} = x n_1 I + n_2 I, \tag{1}$$

$$I_{\text{off}} = n_1 I + n_2 I, \tag{2}$$

where n_1 is the number of Ag atoms in substitutional sites with a neighboring Ag atom in the overlying hollow site (case (iii)), n_2 the number of Ag atoms in hollow sites (case (i)). x represents the enhancement factor of the photoelectron intensity due to forward focusing along ⟨101⟩. Note that inclusion or exclusion of case ii can be compensated with a modified x value. For n_1 in units of a ML we find:

$$n_1 = \frac{I_{\langle 101\rangle} - I_{\text{off}}}{I_{\text{off}}(x-1)} \cdot \text{ML}. \tag{3}$$

$I_{\langle 101\rangle}$ and I_{off} can be determined from azimuthal cuts through the ⟨101⟩ forward focusing peaks. x can be estimated by means of SSC calculations. We find that the intensity in the forward-focusing direction is approximately twice as large as in the other directions, i.e., $x \approx 2$. The results obtained with this model are shown in Fig. 5b. For the lowest Ag coverage, 1% of Cu surface atoms are substituted by Ag atoms. This amount corresponds to 25% of the deposited Ag! With increasing Ag coverage the number of substituted Cu atoms increases. At $\Theta = 0.35$ ML, 15% of the deposited Ag is substitutionally adsorbed, which is equivalent to 5.25% of a Cu layer. Since x is estimated from calculations, and since we neglected the type (ii) Ag atoms our result has only semi-quantitative character: when a diffusing Ag atom (case (i)) meets a substituted Ag atom (case (ii)) it can be trapped in the overlying hollow site. By this process a type (ii) Ag atom becomes a type (iii) Ag atom. As a consequence one observes an increase of $I_{\langle 101\rangle}$, hence, an increase of n_1, although the total number of substituted Ag atoms (case (ii) + case (iii)) remains unchanged. Therefore we do not know if the total number of substituted Ag atoms is increasing continuously with coverage, or if substitution occurs only at the very beginning of the Ag deposition.

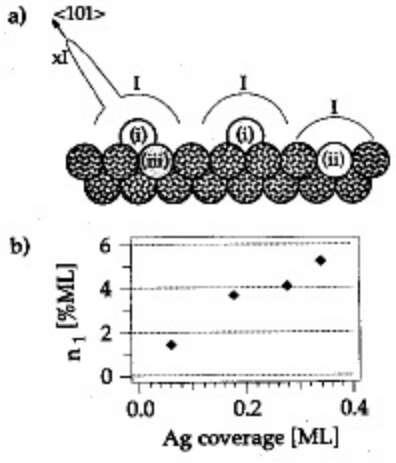

Fig. 5. (a) For $\Theta < 0.75$ ML there are essentially three kinds of Ag atoms at the surface: (i) Ag atoms in hollow sites, (ii) Ag atoms in substitutional sites and (iii) Ag atoms in substitutional sites with a Ag atom in the overlying hollow site. We suppose that the intensity, I, of the spherical waves emitted by these three kinds of Ag atoms is equal. (b) Number of Ag atoms substituted into the first Cu(001) layer, n_1, in units of one Cu(001) layer.

At first sight the formation of such a surface-confined alloy is rather surprising. On the one hand Ag and Cu are immiscible at RT [13, 14]; on

the other hand, as reported in [22], there is no experimental evidence for the existence of such a surface alloy for this system up to now. Referring to this, however, we have to pay attention to the theoretical studies of Tersoff [11] and Foiles et al. [40]. As discussed in the introduction, Tersoff showed with simple considerations based on surface energy, interface energy and strain energy, that such surface-confined mixing is expected quite generally in systems which are dominated by a large LM. Using the embedded-atom method, Foiles calculated the energy of a single Ag atom in the first and in the second atomic layer of the Cu(001) surface relative to the energy of the Ag atom in the bulk of a Cu(001) crystal. According to this calculation Ag is enriched in the first Cu(001) layer and a very small number of Ag atoms may even substitute into the second Cu layer! This is consistent with the interpretation of the faint maxima along ⟨101⟩ as due to Ag emitters within the second Cu layer, and would be the first experimental confirmation of Foiles predictions. Taking into account defects of the Cu(001) surface, one can give an alternative explanation for the formation of a surface-confined alloy. For instance it is known that defect densities on metal surfaces can be as high as a few percent of a monolayer [41]. "Surface alloy" formation might therefore also proceed through filling of vacancies instead of direct substitution of a surface atom.

While for very thin Ag films ($\Theta < 0.3$ ML) neither XPD nor LEED revealed any differences in the structures of the adlayers deposited on the two differently cut Cu(001) crystals, a detailed analysis of all XPD and LEED patterns corresponding to a coverage between 0.3 and 0.75 ML indicates that on the **Cu*(001)** crystal the [110]-domain of the c(10 × 2) structure is dominant. On the **Cu(001)** crystal, however, both orientations are present in more or less equal partitions. A similar behavior has already been observed for Au deposition on the same crystals [4,5]. This statement is visualized in the "2s.npa" representation of the diffractograms from 0.5 ML Ag/Cu*(001) (Fig. 6a) and 0.55 ML Ag/Cu(001) (Fig. 6b) respectively.

We tried to quantify the population of the two domains by means of an *R*-factor analysis [5]. An *R*-factor, R_{MP}, based on the space of multipole expansion coefficients, a_{lm}, of the diffractograms was used to judge the comparison between experimental diffraction data and theory [28,42]. R_{MP} is obtained by summing the distance between the points in the complex plane representing the experimental and theoretical multipole coefficients a_{lm} over all l's and m's considered ($l_{max} = 60$). The theoretical diffractogram $T(c_{[110]}, c_{[\bar{1}10]})$ used to estimate the population of the two c(10 × 2) orientations is a linear combination of the data resulting from the SSC calculations for the [110]-domain ($D_{[110]}$) and the [$\bar{1}$10]-domain ($D_{[\bar{1}10]}$):

$$T(c_{[110]}, c_{[\bar{1}10]}) = c_{[110]} D_{[110]} + c_{[\bar{1}10]} D_{[\bar{1}10]}, \qquad (4)$$

where $c_{[110]}$ and $c_{[\bar{1}10]}$ are the population concentrations normalized to unity. To optimize $c_{[110]}$ and $c_{[\bar{1}10]}$ we used Powell's method to minimize multidimensional functions [43] with starting values of $c_{[110]} = c_{[\bar{1}10]} = 0.5$. In Figs. 6c and 6d the best-fit population coefficients are plotted versus Ag coverage. On the **Cu(001)** crystal the population of both domains is nearly equal. On the **Cu*(001)** crystal, however, the population of the [110]-domains strongly increases with coverage. At a coverage of 0.5 ML about 60% of the Ag atoms are found in [110]-domains. We believe that this preferred occupation of [110]-domains is caused by the course of the steps. Taking into account the supposed shape of the steps shown in Fig. 1, one concludes that the growth of c(10 × 2) domains with Ag rows running parallel to the step edges is favored.

3.2. Thicker films (0.75 ML < Θ < 14 ML)

Thick Ag films, deposited on Cu(001) crystals, are known to have a Ag(111)-like structure [6,12,20,22]. The c(10 × 2) layer at lower coverage represents an ideal template for fcc (111) growth through its quasi-hexagonal topology. In principle, on each of the two c(10 × 2) domains fcc (111) growth can occur in two different orientations which are rotated by 180° with respect to each other. Hence the formation of four fcc (111) domains, rotated by 90° with respect to each other is expected. According to Fig. 7 we label the four fcc (111) domains from 1 to 4. Domains 2 and 4 develop on the [110]-c(10 × 2) template, domains

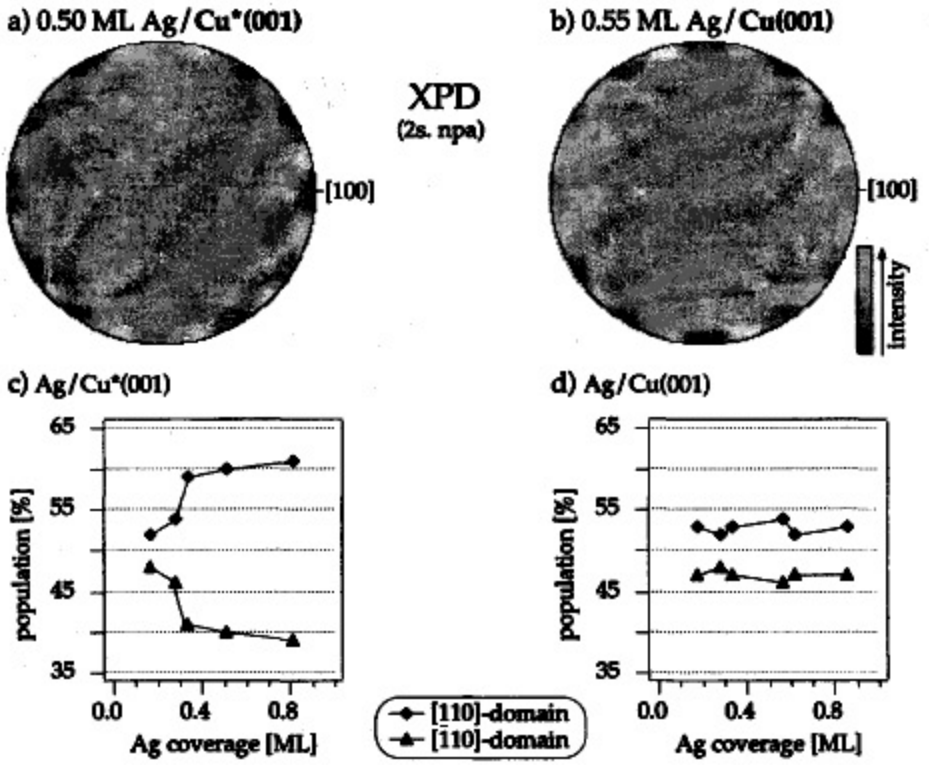

Fig. 6. Stereographic projection of Ag $3d_{5/2}$ diffractograms (E_{kin} = 1371.9 eV) in the "2s.npa" representation of (a) 0.50 ML Ag/**Cu*(001)** and (b) 0.55 ML Ag/**Cu(001)**. Population of the two c(10 × 2) orientations as a function of the Ag coverage for Ag deposited on (c) **Cu*(001)** and (d) **Cu(001)**.

1 and 3 on the [$\bar{1}$10]-c(10 × 2) template. Notice that the orientation of the fcc (111) stereographic projection, shown in Fig. 2b, is chosen such that it corresponds to domain 2.

In Figs. 8a and 8b we present the Ag $3d_{5/2}$ diffractograms from 0.82 ML and 8.2 ML thick Ag films, respectively, deposited on **Cu*(001)**. A comparison of the diffractograms with Figs. 2 and 7 shows that the observed maxima can be identified with the low-index directions and high-density planes of a fcc (111) crystal, oriented like domain 2. Obviously, on this crystal, the growth of domain 2 is predominant. The corresponding LEED pattern is shown in Fig. 8c. On **Cu(001)**, however, we observe the development of domain 2 *and* domain 3. This can be seen, if one analyses carefully Figs. 8d and 8e, where the Ag $3d_{5/2}$ diffractograms of 0.86 and 8.9 ML thick Ag films deposited on **Cu(001)** are shown. LEED also confirms the differences between the two crystals. For thick Ag films on **Cu*(001)** (Fig. 8c) the LEED pattern exhibits twelve spots with three dominant ones, while thick films deposited on **Cu(001)** (Fig. 8f) exhibit six more intense and six weaker reflexes. A similar behavior has been observed for Au deposition onto the same crystals [4,5]. As mentioned above, four equivalent possibilities of fcc (111) growth exist, but in reality they are not equally populated. We found that for 0.55 ML thick Ag films deposited on **Cu(001)** the two c(10 × 2) domains are nearly equally populated, while after deposition of 0.50 ML Ag on **Cu*(001)** about 60% of the Ag atoms are found in the c(10 × 2)-[110]-domain. We conclude therefore, that on the [110]-c(10 × 2) template only domain 2 develops, while on the [$\bar{1}$10]-c(10 × 2) template only domain 3 starts to grow.

To simulate the very beginning of the fcc (111) growth of domain 2 by means of SSC calculations we prepared a cluster according to the top left of

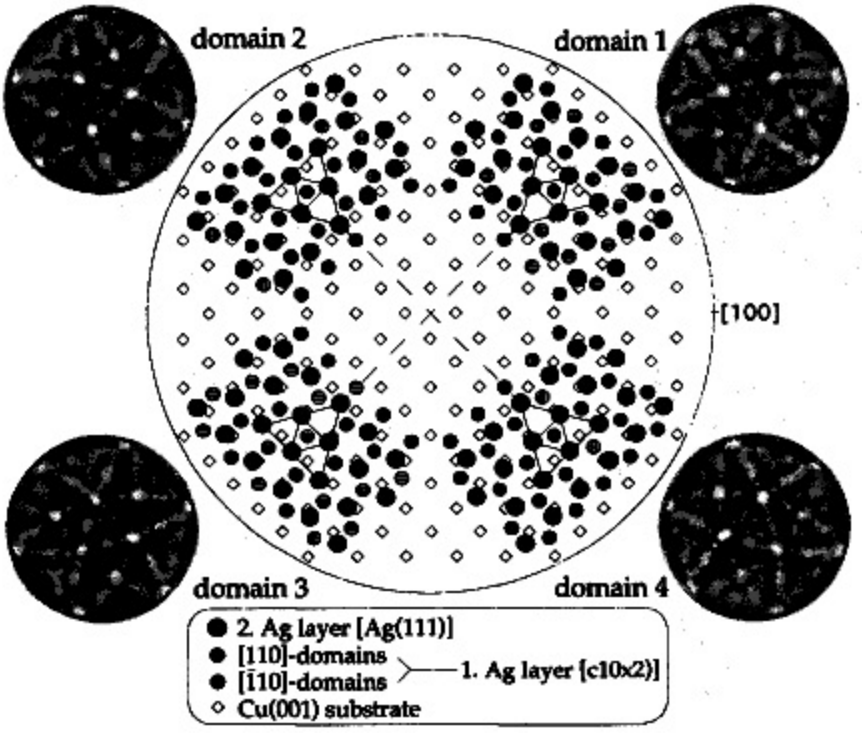

Fig. 7. The four possible fcc (111) domains (see text). For each domain the result of a SSC calculation, using a 8 Ag layer thick film, is shown.

Fig. 7. With this cluster we were able to reproduce the maxima observed in the experiment (Fig. 8a). However, in order to obtain the line of enhanced intensity running like the (100) plane drawn in bold in Fig. 2b, we had to take into account the nine inequivalent positions of the substitutionally adsorbed Ag atoms with respect to the c(10 × 2) structure. We added up to 8 Ag layers one layer after the other, respecting the *abc* stacking of fcc (111) crystals, and performed SSC calculations (not shown). For each thickness the agreement with the experimental diffractograms taken from Ag films with corresponding thickness deposited on **Cu*(001)** is very good.

Compared to a Ag(111) surface the first quasi-hexagonal c(10 × 2) Ag layer is quite distorted. A detailed analysis of all LEED patterns as a function of thickness shows that the Ag layers following the c(10 × 2) layer are still stressed, but, with increasing Ag coverage the lattice constant of the adlayer tends to approach that of the Ag-bulk lattice.

Analyzing the growth mode it is useful to monitor the presence of forward-focusing peaks corresponding to the low-index directions of a fcc (111) crystal (see Figs. 2b and 9) as a function of Ag coverage. In Table 1 where the thickness of the Ag films is given in units of a single Ag(111) layer we compare the appearance of different forward-focusing maxima for an ideal layer-by-layer growth of a fcc (111) film with the experimental observation. Only shortly before the first c(10 × 2) Ag layer is completed do we observe peaks due to emitters in a second Ag layer. Therefore, the first layer seems to be completed before the second starts to grow. For further deposition we observe the formation of low-index directions which should be present only after the completion of the second respectively the third layer in the case of ideal layer-by-layer growth. Thus, this is an indication for the growth mode to be of the SK type, agreeing with ISS observations by Nakanishi et al. [22]. Compared to the reports of other authors [20,23,25] and considering the surface energies

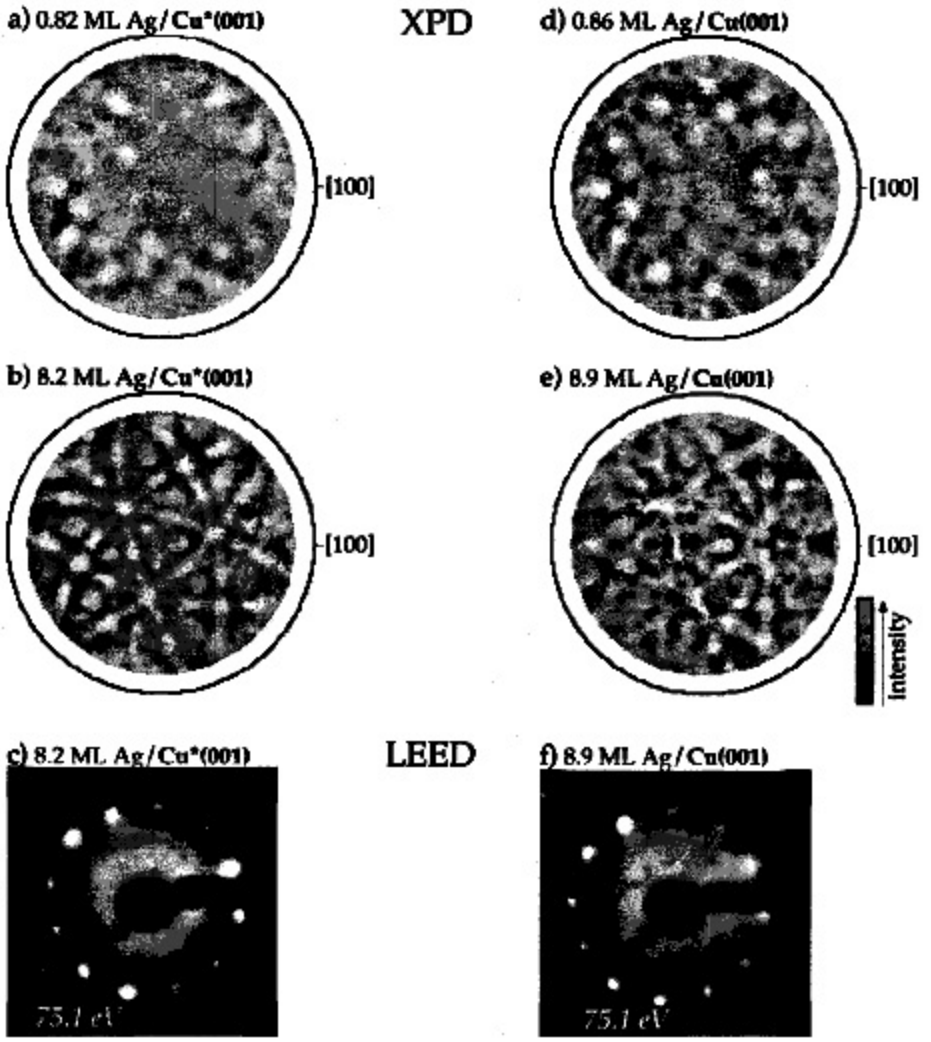

Fig. 8. Ag deposited on Cu*(001): Stereographic projection of Ag $3d_{5/2}$ diffractograms (E_{kin} = 1371.9 eV) in the "rc80.npa" representation of a (a) 0.82 ML, (b) 8.2 ML thick Ag film. (c) LEED pattern of a 8.2 ML thick Ag film. Ag deposited on Cu(001): Stereographic projection of Ag $3d_{5/2}$ diffractograms (E_{kin} = 1371.9 eV) in the "rc80.npa" representation of a (d) 0.86 ML, (e) 8.9 ML thick Ag film. (f) LEED pattern of a 8.9 ML thick Ag film.

($\gamma_{Ag} \ll \gamma_{Cu}$), both arguing for the FM growth mode, our finding is surprising. Two arguments support our result: first, XPD and ISS yield direct information on the local structure of the surface, while the authors of Refs. [20,23,25] argue with intensity ratios of photo- or Auger electrons. Second, the interface energy has to be taken into account. The distortion of the Ag film, which is important after the first layer and reduces with each successive layer, introduces an important positive interface energy into the Young equation. In order to reduce this interface energy, Ag atoms possibly prefer to form a new layer before finishing the previous one. A limited interlayer mass transport could be an alternative explanation for the observed growth mode. During the growth of Ag on Ag(111) – this situation is almost equivalent with the growth of Ag on the quasihexagonal c(10 × 2) overlayer – this phenomenon leads to the formation of three dimensional islands [44]. Note that, as already discussed in Ref. [6], thick Ag films are nevertheless compact, i.e., cover the substrate completely.

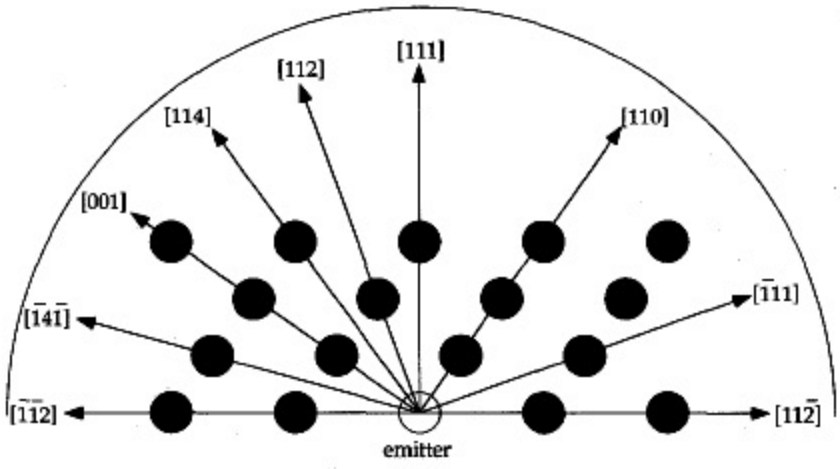

Fig. 9. Polar cut from [11$\bar{2}$] to [$\bar{1}\bar{1}$2] showing the principal low-index directions present in the first four monolayers of a fcc (111) crystal.

Table 1
Appearance of the forward-focusing peaks corresponding to the low-index directions of a fcc (111) crystal (see Figs. 2b and 9) as a function of the thickness of the deposited Ag film

Low-index directions	⟨001⟩	⟨011⟩	⟨11$\bar{1}$⟩	⟨$\bar{1}\bar{1}$4⟩	⟨112⟩	⟨114⟩	⟨111⟩
	peak visible after completion of layer #:						
Ideal fcc (111) layer-by-layer growth	1	1	1	1	2	3	3
Ag/**Cu*(001)**	0.90	0.90	0.90	0.90	1.83	2.47	2.47
Ag/**Cu(001)**	0.96	0.96	0.96	0.96	1.80	2.40	2.40

We tried to estimate the population of the four possible Ag(111) domains as a function of thickness from 2 to 8 layers by means of a *R*-factor analysis as already described above. Here, the theoretical diffractograms $T^k(c^k)$ with $c^k = (c_1^k, c_2^k, c_3^k, c_4^k)$ are linear combinations of the four Ag(111) domains $(D_1^k, D_2^k, D_3^k, D_4^k)$ taken first from the SSC calculations of $k = 2, 3, \ldots, 8$ layer thick Ag films, and then also from an experimental Pt $4d_{5/2}$ diffractogram ($E_{kin} = 1430.4$ eV) of a Pt(111) single crystal (labeled with $k = 11$) representing an ideal bulk fcc (111) structure. The choice $k = 11$ is arbitrary and just serves to represent the results of the fits. The c_i^k are the population coefficients of the corresponding domains and are normalized to unity:

$$T^k(c^k) = \sum_{i=1}^{4} c_i^k D_i^k. \qquad (5)$$

For all Ag $3d_{5/2}$ diffractograms taken from Ag films thicker than 0.75 ML we determined the minimal *R*-factor R_{MP}^k for each k and plotted it versus k. In such a manner we obtained for all films the k value (thickness) for which R_{MP}^k is minimal and from the corresponding c_i^k the population of the four possible Ag(111) domains. The population distribution of the best fits versus the Ag coverage is shown in Figs. 10a and 10b. As an example, the result of the fit for a 8.2 ML thick film on **Cu*(001)** is shown in Fig. 10c, the one for a 8.9 ML thick film on **Cu(001)** in Fig. 10d. The agreement with the experiment (Figs. 8b and 8e) is excellent. Above a coverage of 4 ML the population of the four domains remains more or less constant. On **Cu*(001)** domain 2 is dominant (75%,) domain 3 is present with 25%, but domains 1 and 4 are no longer observed. This is consistent with the result of a similar fit performed by

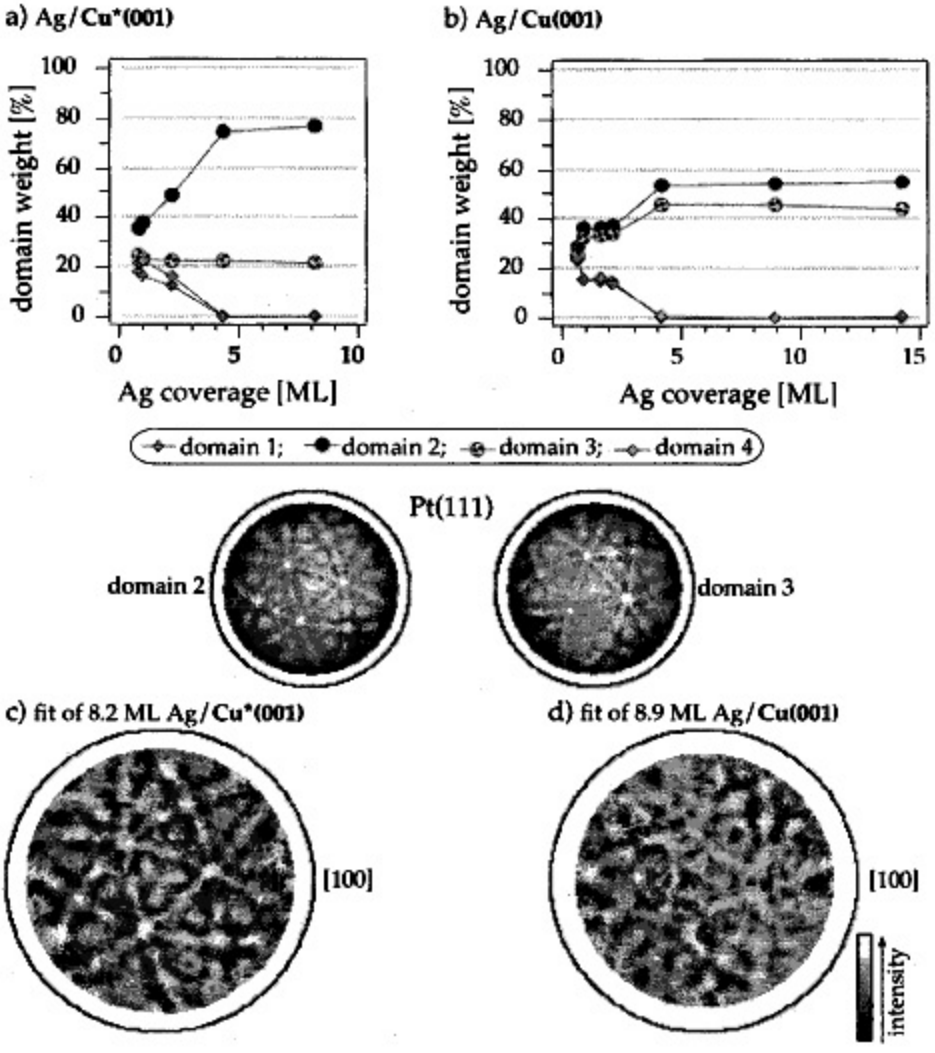

Fig. 10. Population of the four possible Ag(111) domains for Ag deposited on (a) **Cu*(001)**, (b) **Cu(001)**. The experimental Pt $4d_{5/2}$ diffractogram (E_{kin} = 1430.4 eV) of a Pt(111) single crystal used for the fit is shown in the "rc80.npa" representation and oriented like domains 2 and 3. Fit with (c) 8.2 ML Ag/**Cu*(001)**, (d) 8.9 ML Ag/**Cu(001)** in the "rc80.npa" representation.

Naumović et al. [5,6] for a 8 ML thick Ag film deposited on **Cu*(001)**. On **Cu(001)** domains 1 and 4 do not grow either, while domain 2 is populated with 55% and domain 3 with 45% of the deposited Ag.

3.3. Conceivable influence of the steps on the Ag growth

To conclude we discuss the conceivable influence of the steps on the Ag growth. Note that the following considerations are based on the assumption that the shape of the steps for both Cu(001) samples is as proposed in Fig. 1.

As discussed in Section 3.1., we find that the growth of c(10 × 2) clusters with their non-primitive unit cell, i.e, with Ag rows running parallel to the step edges, is favored. We think that a Ag cluster which grows in the center of a terrace chooses arbitrarily one of the two possible c(10 × 2) orientations, while the non-primitive c(10 × 2) unit cell of a Ag cluster growing at the

downhill side of a step edge is always parallel to the step edge. The following geometric arguments support this statement: In Figs. 11a and 11b one sees a c(10×2) Ag cluster with its non-primitive unit cell parallel ([110]-domain), respectively, perpendicular ([1$\bar{1}$0]-domain) to the step edge of a step ascending along [1$\bar{1}$0]. Obviously, only for the [110]-domain is the border between the c(10×2) Ag adlayer and the step compact. In the case of the [1$\bar{1}$0]-domain this border is serrated. Ag has a much smaller surface energy (γ) than Cu ($\gamma_{Ag} \ll \gamma_{Cu}$). Ag atoms therefore tend to wet the step edges, i.e., they try to go as close as possible to the steps. Thus, having a step ascending along [1$\bar{1}$0] results in the formation of a [110]-domain. Therefore, for the following fcc (111) growth, one already can exclude the formation of domain 1 and domain 3 (Fig. 7).

As shown in Fig. 1, we expect the steps to ascend in the [1$\bar{1}$0] direction on the **Cu*(001)** crystal. The result of our *R*-factor fit for a 8.2 ML thick Ag film deposited on **Cu*(001)** shows that, on this crystal, 75% of the Ag populates domain 2. We conclude that, steps ascending along [$\bar{1}\bar{1}$0]/[1$\bar{1}$0]/[110]/[$\bar{1}$10] would result in the formation of domain 1/domain 2/domain 3/domain 4 respectively. The following geometric arguments support this statement: In Table 1 one sees that only shortly before the c(10×2) Ag layer is completed does the second Ag layer starts to grow. At the corresponding coverage the border between the c(10×2) Ag adlayer and the step still looks as in Fig. 11a. In order to reduce the wetting energy, successively deposited Ag atoms tend to wet the not yet covered parts of the Cu surface ($\gamma_{Ag} \ll \gamma_{Cu}$). On the other hand, due to the smaller interface energy, the deposited Ag atoms prefer to be adsorbed on the quasi-hexagonal c(10×2) clusters. At the border between the c(10×2) Ag adlayer and the step, both conditions are fulfilled. Thus, the second Ag layer starts to grow at this location. In addition to Fig. 11a we display in Figs. 11c and 11d some Ag rows of the second Ag layer, having a fcc (111) structure. The configuration in Fig. 11c will result in the development of domain 2 (Fig. 7). The situation presented in Fig. 11d will result in the formation of domain 4. One sees that at the border between the c(10×2) Ag adlayer and the step, some second layer Ag atoms of domain 4 would be placed on bridge sites, while some of them would be placed in hollow sites, thus implying a strong corrugation. For domain 2 there exist no such bridge sites. The formation of domain 2 therefore appears energetically favorable compared to the formation of domain 4.

At this point, however, a *direct* confirmation of the influence of the step alignment on the formation of the c(10×2) clusters and of the Ag(111) domains, respectively, is clearly desirable. If the above arguments are confirmed, intentional misalignment of a crystal could very well provide a means of selectively preparing single c(10×2) and Ag(111) domain structures, respectively, which warrants further investigations.

4. Conclusions

For the initial stage of Ag growth, XPD indicates the formation of a surface alloy. For the lowest Ag coverage of 0.04 ML, approximately 1% of the Cu atoms of the top Cu layer and even a very small number of Cu atoms of the second Cu layer may be substituted by Ag. This value increases to 5% at a coverage of 0.35 ML. SSC calculations suggest that most of the deposited Ag atoms diffuse over the surface until they get trapped at the downhill side of the step edges, or, until they meet a substituted Ag atom and are trapped in one of the overlying hollow sites. At Ag coverages around 0.20 ML the formation of c(9×9) clusters which are very corrugated, and therefore unstable, is proposed. In order to reduce corrugation the Ag atoms slide along ⟨110⟩ directions and rows of Ag atoms are formed along these directions during further Ag deposition. Through this process, compact c(10×2) clusters are formed, occurring in two domains. XPD indicates a c(10×2) local atomic arrangement already at a coverage of 0.3 ML. Moreover, we find clear evidence that the formation of c(10×2) clusters occurs preferentially with Ag rows running parallel to the steps. Compared to the hexagonal Ag(111) surface the quasi-hexagonal c(10×2) layer is distorted. During the growth of Ag(111) domains, which

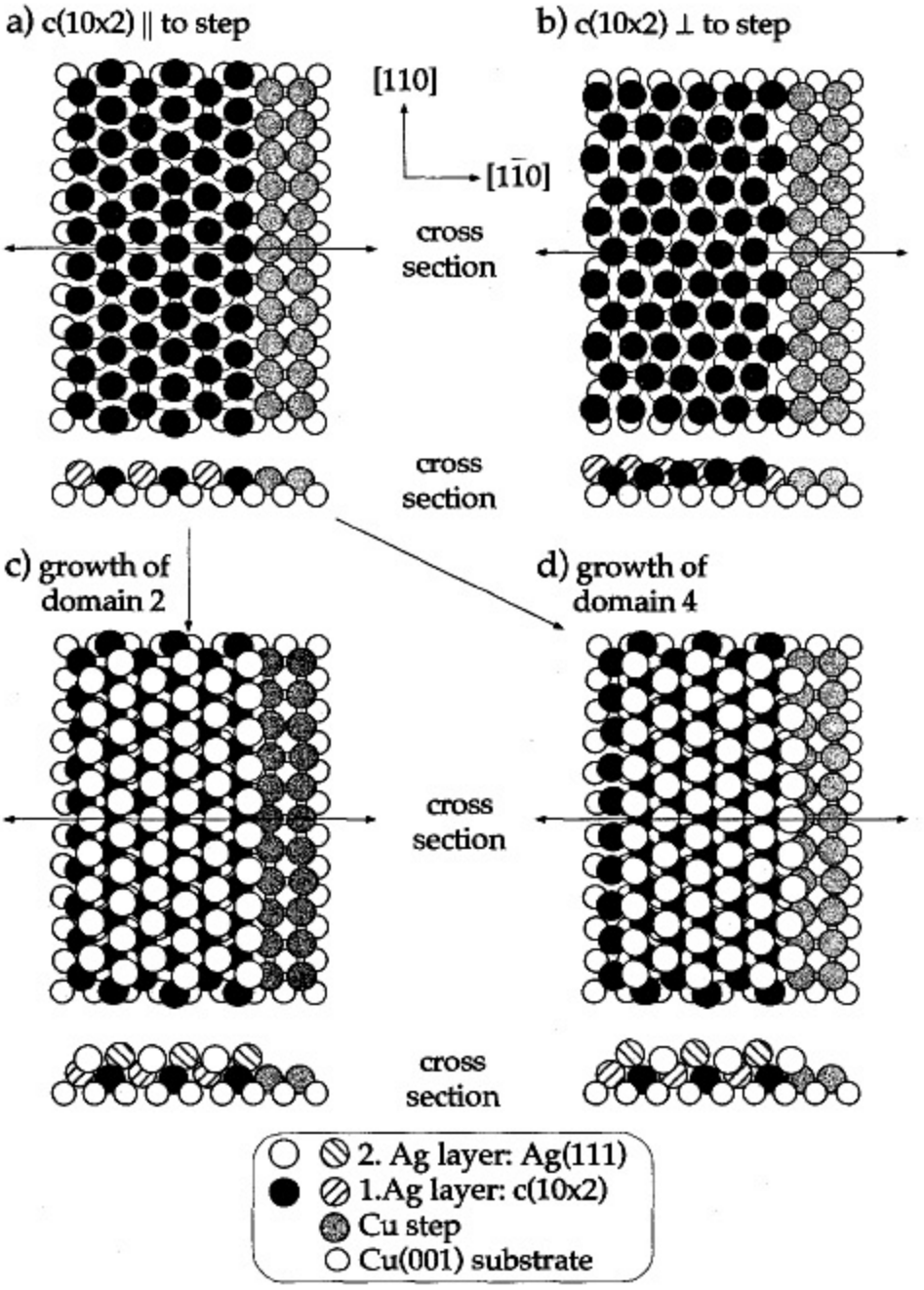

Fig. 11. c(10 × 2) cluster with its non-primitive unit cell (Ag rows) (a) parallel ([110]-domain), (b) perpendicular ([1$\bar{1}$0]-domain) to a Cu-step ascending along [1$\bar{1}$0]. Second Ag layer [Ag(111)] on the [110]-domain resulting in the growth of (c) domain 2, (d) domain 4. The double-arrows mark the cross-section; streaked Ag atoms in the cross-sections always represent atoms behind the cross-section planes.

starts shortly before the completion of the first Ag layer, this distortion decreases. There are two possibilities of fcc (111) growth on each c(10 × 2) domain, but only one is observed. Thus, only two fcc (111) domains rotated by 90° with respect to each other develop. The comparison of the results from the two differently cut crystals indicates that the domain population is related to the absolute miscut of the substrate and hence by the course of the steps.

Acknowledgements

We profited from stimulating discussions with R.G. Agostino and J. Osterwalder. Skillful technical assistance was provided by F. Bourqui, E. Mooser, O. Raetzo and H. Tschopp. This project has been supported by the Fonds National Suisse pour la Recherche Scientifique.

References

[1] E. Spiller, in: Physics, Fabrication and Applications of Multilayered Structures, Eds. P. Dhez and C. Weisbuch (Plenum, New York, 1988).
[2] T. Shinjo, N. Hosoito, K. Kawaguchi, N. Nakayama, T. Takada and Y. Endoh, J. Magn. Magn. Mater. 54–57 (1986) 737, and references therein.
[3] C.M. Falco and L.K. Schuller, Synthetic Modulated Structures/VLSI, Eds. L.I. Chang and B.C. Grissen (Academic Press, New York, 1985); P. Houdy, Met. Multilayers, Trans. Tech. Pub. 59/60 (1990) 581; P. Beccat and J. Massardier, Catal. Lett. 9 (1991) 183.
[4] D. Naumović, A. Stuck, T. Greber, J. Osterwalder and L. Schlapbach, Surf. Sci. 269/270 (1992) 719; 277 (1992) 235 (Erratum); 287/288 (1993) 950.
[5] D. Naumović, PhD Thesis, University of Fribourg, Switzerland, 1993.
[6] D. Naumović, P. Aebi, A. Stuck, P. Schwaller, J. Osterwalder and L. Schlapbach, Surf. Sci. 307–309 (1994) 483.
[7] H. Röder, R. Schuster, H. Brune and K. Kern, Phys. Rev. Lett. 71 (1993) 2086.
[8] J. Neugebauer and M. Scheffler, Phys. Rev. Lett. 71 (1993) 577; J. Burchhardt, M.M. Nielsen, D.L. Adams, E. Lundgren, J.N. Andersen, C. Stampfl, M. Scheffler, A. Schmalz, S. Aminpirooz and J. Haase, Phys. Rev. Lett. 74 (1995) 1617.
[9] L.P. Nielsen, F. Besenbacher, I. Stensgaard, E. Lægsgaard, C. Engdahl, P. Stoltze, K.W. Jacobsen and J.K. Nørskov, Phys. Rev. Lett. 71 (1993) 754.
[10] S. Oppo, V. Fiorentini and M. Scheffler, Phys. Rev. Lett. 71 (1993) 2437.
[11] J. Tersoff, Phys. Rev. Lett. 74 (1995) 434.
[12] P.W. Palmberg and T.N. Rhodin, J. Chem. Phys. 49 (1968) 134, 147; J. Appl. Phys. 39 (1968) 2425.
[13] M. Hansen and K. Anderko, Constitution of Binary Alloys (McGraw- Hill, New York, 1958); J.L. Murray, Metall. Trans. A 15 (1984) 261.
[14] G. Gladyszewski and Z. Mitura, Surf. Sci. 231 (1990) 90.
[15] A. Saúl, B. Legrand and G. Tréglia, Phys. Rev. B 50 (1994) 1912; Surf. Sci. 331–333 (1995) 805.
[16] A. Senhaji, G. Tréglia, J. Eugène, A. Khoutami and B. Legrand, Surf. Sci. 287/288 (1993) 371.
[17] J. Eugène, B. Aufray and F. Cabané, Surf. Sci. 241 (1991) 1; 273 (1992) 372.
[18] G. Tréglia, B. Legrand, J. Eugène, B. Aufray and F. Cabané, Phys. Rev. B 44 (1991) 5842.
[19] Y. Liu and P. Wynblatt, Surf. Sci. 240 (1990) 245; 241 (1991) L21; 290 (1993) 335; 310 (1994) 27.
[20] J.G. Tobin, S.W. Robey, L.E. Klebanoff and D.A. Shirley, Phys. Rev. B 28 (1983) 6169; 35 (1987) 9056; 33 (1985) 2270.
[21] A.P. Shapiro, T.C. Hsieh, A.L. Wachs, T. Miller and T.-C. Chiang, Phys. Rev. B 38 (1988) 7394.
[22] S. Nakanishi, K. Kawamoto and K. Umezawa, Surf. Sci. 287/288 (1993) 974.
[23] J.E. Black, D.L. Mills, W. Daum, C. Stuhlmann and H. Ibach, Surf. Sci. 217 (1989) 529.
[24] J.E. Black and Z.-J. Tian, Surf. Sci. 291 (1993) 215.
[25] C. Mottet, G. Tréglia and B. Legrand, Phys. Rev. B 46 (1992) 16018.
[26] E. Bauer, Surf. Sci. 7 (1967) 351.
[27] J. Osterwalder, T. Greber, A. Stuck and L. Schlapbach, Phys. Rev. B 44 (1991) 13746; D. Naumović, A. Stuck, T. Greber, J. Osterwalder and L. Schlapbach, Phys. Rev. B 47 (1993) 7462.
[28] R. Fasel, P. Aebi. J. Osterwalder and L. Schlapbach, Surf. Sci. 331–333 (1995) 80; Phys. Rev. B 52 (1995) R2313; 50 (1994) 14516.
[29] C.S. Fadley, in: Synchrotron Radiation Research: Advances in Surface Science, Ed. R.Z. Bachrach (Plenum, New York, 1990).
[30] W.F. Egelhoff Jr., Crit. Rev. Solid State Mater. Sci. 16 (1990) 213.
[31] S.A. Chambers, Adv. Phys. 40 (1991) 357.
[32] M. Poensgen, J.F. Wolf, J. Frohn, M. Griesen and H. Ibach, Surf. Sci. 274 (1992) 430.
[33] D.D. Chambliss and S. Chiang, Surf. Sci. 264 (1992) L187.
[34] D.J. Friedman and C.S. Fadley, J. Electron Spectrosc. Relat. Phenom. 51 (1990) 689.
[35] Seah and Dench, Surf. Interface Anal. 1 (1979) 2.
[36] D.C. Jackson, T.E. Gallon and A. Chambers, Surf. Sci. 36 (1973) 381.
[37] R.L. Gerlach and T.N. Rhodin, Surf. Sci. 10 (1968) 446.
[38] D.D. Chambliss and K.E Johnson, Phys. Rev. B (1994) 5012.

[39] W.E. McMahon, E.S. Hirschorn and T.-C. Chiang, Surf. Sci. 279 (1992) L231.
[40] S.M. Foiles, M.I. Baskes and M.S. Daw, Phys. Rev. B 33 (1986) 7983.
[41] J.N. Andersen, E. Lundgren, R, Nyholm and M. Qvarford, Surf. Sci. 289 (1993) 307.
[42] J. Osterwalder, R. Fasel, A. Stuck, P. Aebi and L. Schlapbach, J. Electron Spectrosc. Relat. Phenom. 68 (1994) 1.
[43] W.H. Press, B.P. Flammery, S.A. Teukosky and W.T. Vetterling, Numerical Recipies, The Art of Scientific Computing (Cambridge University Press, 1986).
[44] K. Bromann, H. Brune, H. Röder and K. Kern, Phys. Rev. Lett. 75 (1995) 677.